



Optical and mechanical studies on free standing amorphous anodic porous alumina formed in oxalic and sulphuric acid

P. Ramana Reddy^{1,2} · K. M. Ajith² · N. K. Udayashankar²

Received: 12 June 2018 / Accepted: 5 October 2018 / Published online: 22 October 2018
© Springer-Verlag GmbH Germany, part of Springer Nature 2018

Abstract

Anodic porous alumina (APA) membranes with a uniform pore arrangement typically serve as an ideal template for formation of different types of nanostructured materials. In the present work, APA membranes were synthesized using two-step anodization in 0.3 M of oxalic and 0.3 M of sulphuric acid under the anodization potential of 40 V and 20 V respectively, at 8 °C. Alumina nanowires (ANW) were synthesized by the chemical etching of the APA membranes using phosphoric acid solution. The optical absorbance and reflectance measurements of APA membranes were performed on a spectrometer in the wavelength range of 200–600 nm. The band-gap energy (3.7 and 4.3 eV for oxalic and sulphuric acid) of APA membranes was determined from UV–visible absorption data. The photoluminescence (PL) investigations have revealed the presence of F and F⁺ defect centers, which could be attributes to oxygen vacancy-related defect centers in oxalic (483 and 466 nm) and sulphuric (423 and 421 nm) alumina. The mechanical properties of amorphous APA membranes were investigated by micro- and nanoindentation techniques. The results indicate that highest hardness (7.70 GPa) and Young's modulus (138.80 GPa) for sulphuric alumina compared with oxalic alumina. In sulphuric alumina, more number of ANW were observed compared with oxalic alumina.

1 Introduction

Self-organized anodic porous alumina (APA) membranes prepared using two-step anodization in acidic electrolytes [1] have been employed as templates for the fabrication of nanostructures [2], such as nanoparticles [3], nanowires [4, 5] nanorods and nanotubes [6], optoelectronic and electronic systems [7], because of their chemical, thermal stability, and high aspect ratio of pores. APA is economically viable to prepare and have a high pore density compared with carbon nanotubes and polymers fabricated using lithographic techniques [8]. It is well known that, the pore dimensions and aspect ratio of APA membranes are controllable and can be varied by changing the anodization process parameters [9–11]. In fact, direct template synthesis based on two-step anodization has been extensively used to fabricate

nanomaterials including magnetic materials, quantum dot arrays, and photo-catalysis [12, 13]. Metallic nanowires or nanotubes, uniform in diameter and length, were obtained by depositing appropriate metals inside their nanopores or on their top surface of the APA membranes [14–16]. Even though the preparation of APA membranes using anodization is simple, the optimization of process parameters using different acidic electrolytes is complex [17]. To prepare highly ordered APA membranes, various methods have been performed, like heat treatment, electro polishing, and single- or multi-step anodizing. In addition to synthesis of alumina, the optical properties of the APA membranes were broadly addressed by many authors [18, 19]. It was reported that APA membranes exhibit a strong peak in blue region, when exposed to ultraviolet light [20]. The mechanism behind the light emitting of APA membranes remains complicated, due to large number of defects during the growth of alumina [21]. In general, in anodizing process of APA, membranes result in hardness usually in the range of 4–6 GPa by micro-indentation [22]. In spite of some previous reports on mechanical properties of APA [23], there is sufficient scope for the investigation of how the porous structure of APA and mechanical properties (hardness and Young's modulus) change in deformation process. Some reports exist

✉ P. Ramana Reddy
ramana.nitk@gmail.com

¹ Department of sciences and humanities, VFSTR Deemed to be University, Vadlamudi, Guntur, Andhra Pradesh 52213, India

² Department of Physics, National Institute of Technology Karnataka, Surathkal, Mangalore 575025, India

on the mechanical behavior of APA membranes with aluminium substrates [24]. However, the mechanical properties of free standing APA membranes along with morphological and optical properties were poorly investigated. Hence, in-depth analyses on optical and mechanical properties of APA membranes are essential to use these membranes as templates for the synthesis of nanostructures. In this article, we describe the structural, optical, and mechanical properties of APA membranes obtained in oxalic ($C_2H_2O_4$) and sulphuric (H_2SO_4) acid as electrolytes. The importance of the present work is to study the optical and mechanical properties of APA membranes and to synthesize alumina nanowires on the pore channels of the oxalic and sulphuric alumina by chemical etching method.

2 Materials and methods

2.1 Synthesis of free standing anodic porous alumina membranes

High-purity aluminium foils (Merck, 99.99%), 0.3 mm thickness, were used as a starting material. The aluminium foils were annealed at 500 °C for 5 h under vacuum to obtain a homogeneous pore growth over a large areas [25]. The foils were later electropolished in a volume mixture of 1:4 perchloric acid and ethanol under a constant current density of 200 mA cm^{-2} for 2 min at 10 °C. Al foils were anodized in 0.3 M of oxalic and 0.3 M of sulphuric acid at 40 V and 20 V respectively, for 6 h at 8 °C, as the first step, and then immersed in a mixture of 6 wt% H_3PO_4 and 1.8 wt% H_2CrO_4 at 60 °C for 120 min to remove the formed alumina layer. The second-step anodization was performed keeping all the anodizing parameters same as those used in the first step. The remaining aluminium substrate was removed in a saturated solution of hydrochloric acid and copper chloride ($HCl/CuCl_2$) after the second-step anodization. Subsequently, a 5 wt% of phosphoric acid (H_3PO_4) solution was used to perform pore-widening process for 30 min at room temperature [26]. To prepare ANW array, anodization process was carried out in 0.5 M electrolyte concentration, with anodization potential of 40 V and 20 V, for 6 h in both oxalic and sulphuric acid solutions. After the anodization process, APA membranes were etched in 1 M of phosphoric acid for 45 min. Immediately, the formed alumina nanowires were annealed in air for 2 h at 60 °C.

2.2 Characterizations

Scanning electron microscopy (SEM, JEOL-JSM-6380LA, Japan) was used to study the surface morphology of the APA membranes. The elemental composition of alumina membranes was identified by energy-dispersive X-ray (EDAX)

attached with SEM. The structural analysis of APA membranes was studied by X-ray diffractometer (XRD, Rigaku-miniflex-600) with CuK_{α} radiation operated at 40 kV and 15 mA. The optical absorption and reflectance spectra of the APA membranes were measured in the wavelength range 200–600 nm using UV–visible spectrometer (SD 2000, Ocean Optics Inc., USA). Photoluminescence (PL) measurements were performed at room temperature on a Floromax-4 fluorescence spectrometer using Xenon light source with an excitation wavelength of 380 nm. Mechanical properties of APA membranes were carried out by micro-indentation (Clemex micro hardness tester, MMT X7, Matsuzawa Seiki Corp., Japan) and nanoindentation techniques (Hysteron Inc., Minneapolis, USA, TI-900).

3 Results and discussion

Figure 1a, e shows the SEM images of the APA membranes prepared in oxalic and sulphuric acid as electrolyte with an anodization potential of 40 and 20 V, respectively [27]. The surface morphologies of the oxalic and sulphuric alumina exhibited hexagonal porous structure with uniform array of pores shown in Fig. 1. In this work, the average size of the pores of APA membranes was measured using the Image J software [28] and measured pore diameter for oxalic alumina was ~63 nm and that for sulphuric alumina was ~32 nm. Figure 1b, f shows the EDAX spectra of the oxalic and sulphuric alumina. The elemental analysis revealed the presence of Al and O elements in the APA membranes. The average atomic percentages of Al and O are 46.42% and 53.58% in oxalic alumina, whereas, in sulphuric alumina, atomic percentages of Al and O are 40.32% and 59.68%, respectively. Regularity ratio (RR) was performed in Fig. 1a, b, to obtain the quantitative evaluation of hexagonal arrangement of nanopores in APA. RR of APA membranes was calculated using the expression [29], to estimate the regularity RR, radial average was generated from each fast Fourier transform (FFT) image. FFT were generated and taken into further calculations with the WSxM 5.0 software [30]. 2D FFT images (Fig. 1c, g) and their radial averages (Fig. 1d, h) for oxalic and sulphuric alumina, respectively, was shown in Fig. 1. It was observed that, in sulphuric alumina, ordering is poor compared with oxalic alumina. Poor ordering was also confirmed by blurred ring on the FFT image (Fig. 1g) and relatively low intensity of radial average (Fig. 1h) in sulphuric alumina. XRD pattern of the oxalic and sulphuric alumina membranes is shown in Fig. 2. It was noticed that APA membranes obtained in different electrolyte solutions provide a similar trend under the XRD measurements. No sharp diffraction peaks were detected from any particular crystallographic plane of the APA membranes. Therefore, it can be pointed out that the APA membranes fabricated

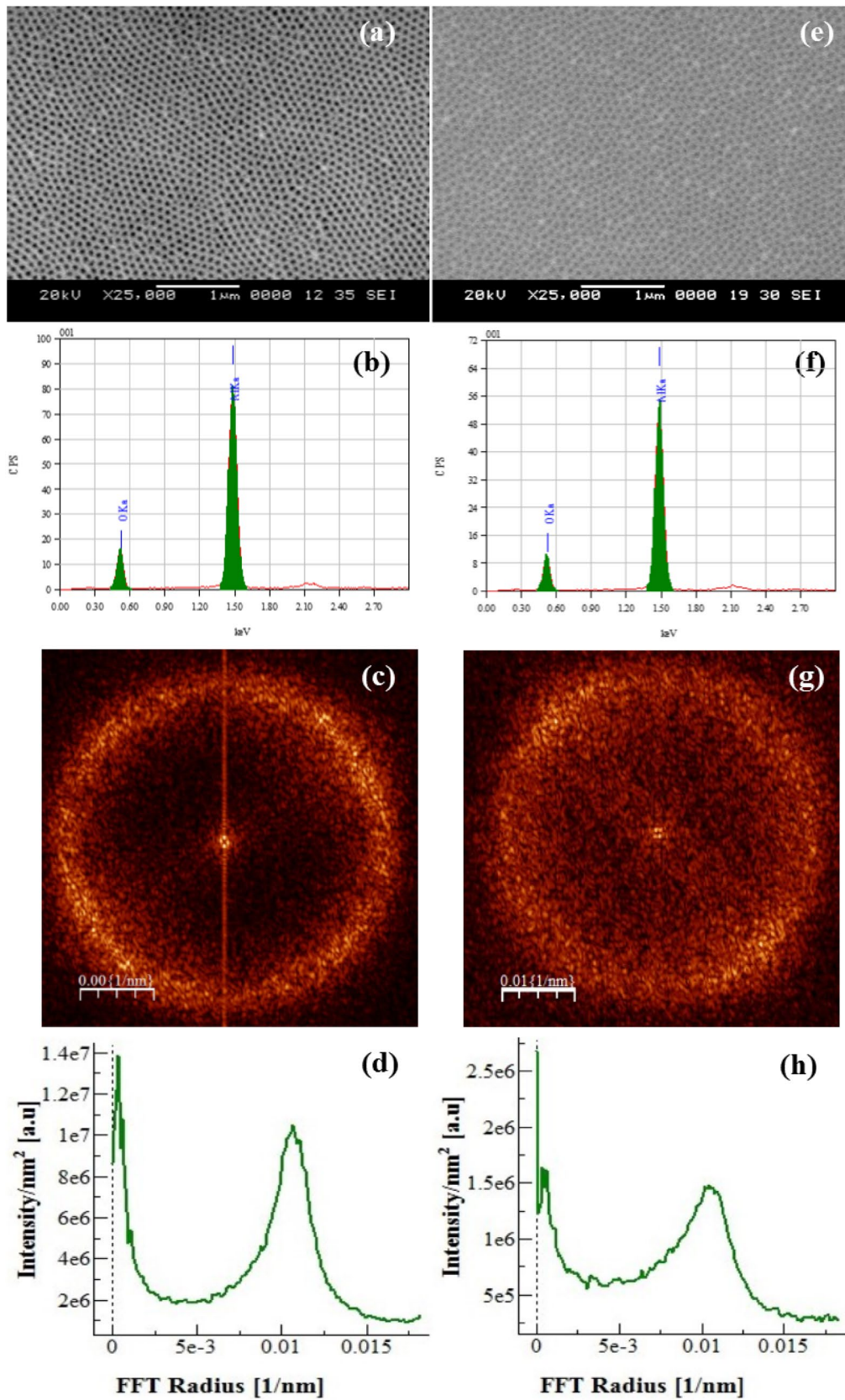


Fig. 1 SEM, EDAX micrographs, 2D FFT images, and radial averages of APA membranes prepared in 0.3 M of oxalic (a–d) and sulphuric acid (e–h)

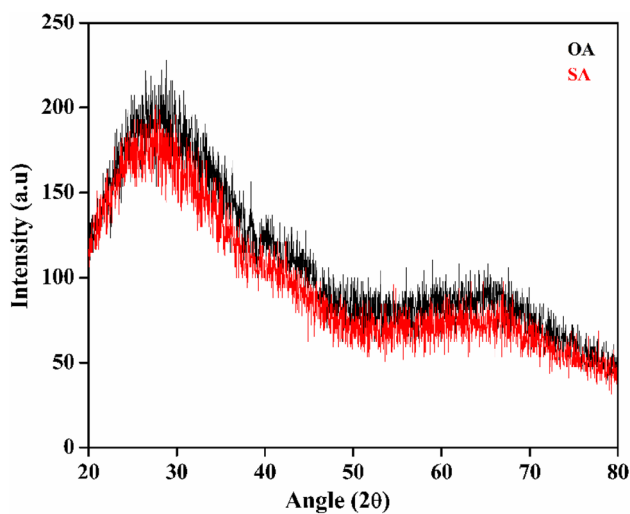


Fig. 2 XRD pattern of APA membranes formed in oxalic and sulphuric alumina

in oxalic and sulphuric acid solutions were amorphous in nature [25].

Figure 3a shows the optical absorption spectra of the oxalic and sulphuric alumina; results indicated that optical absorption is high in oxalic alumina compared with sulphuric alumina. This is due to decrease in defect states and it was clearly visible in Fig. 1. The band-gap energy of APA membranes estimated from UV–visible absorption spectra using the Tauc’s relation [31]. The plot of $(\alpha h\nu)^2$ versus $h\nu$ is shown in Fig. 3b. The calculated band-gap energy values for APA membranes were found to be 3.7 and 4.3 eV for oxalic and sulphuric alumina, respectively. Decrease in band-gap energy in oxalic alumina compared with sulphuric alumina may be due to more absorption defects and oxalic impurities in oxalic alumina [32, 33]. Moreover, the incorporation of cations and anions into oxides

during anodic oxidation of metals also causes the change in the bandgap of oxalic alumina [34, 35]. The reflectance spectra of the APA membranes are shown in Fig. 4. The reflectance increases gradually and smoothly from blue region to red region of the spectrum, and the interference band with maximum reflectance in the visible region shows a red shift in both oxalic and sulphuric alumina. The most significant factor for the red shift is the increase of thickness of APA membranes according to the calculations obtained from Bragg’s relation [36, 37] which indicates that the wavelength of the maximum reflection increases with increasing the film thickness. The reflectance spectrum between 400 and 800 nm is also shown in the Fig. 5 (Inset). Moreover, the coordinates of the APA membranes were estimated using the international commission on illumination (CIE) 1931 [38] and color functions are represented in Fig. 5. The chromaticity coordinates were calculated for oxalic and sulphuric alumina where $x=0.3476$, $y=0.3371$ and $x=0.3476$, $y=0.3369$ correspondingly. The higher intensity reflectance peak was observed in the red region in sulphuric and oxalic alumina. It was also confirmed by the CIE analysis of reflectance spectra for oxalic (Fig. 5a) and sulphuric (Fig. 5b) alumina. The maximum number of interference reflections was more in oxalic alumina compared with sulphuric alumina, due to lower thickness of alumina in sulphuric acid solution. The PL spectra of the APA membranes obtained in oxalic and sulphuric acid electrolytes are shown in Fig. 6. It was pointed out that APA membranes exhibit a broad luminescence in the blue region (300–600 nm). The origin of the PL in APA is still controversial, though it is generally accepted that there are two major reasons for the luminescence behavior of APA membranes [39], (1) F centers, associated with the carboxylic impurities from the acid electrolyte incorporated in the structure of alumina and (2) F^+ centers, which are related to oxygen vacancy-related defect centers present in the APA membranes. To study the dependence of blue PL band on

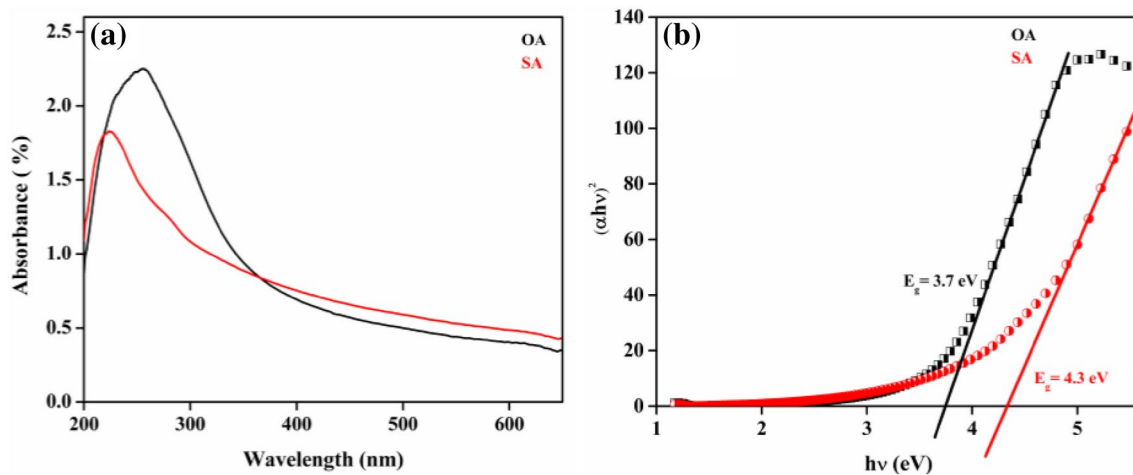


Fig. 3 UV–visible absorption spectra (a) and plot of $(\alpha h\nu)^2$ versus $h\nu$ (eV) of APA membranes for oxalic and sulphuric alumina

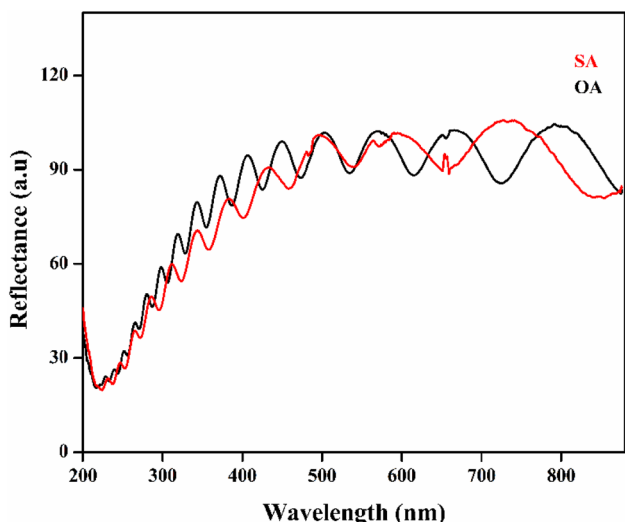


Fig. 4 Reflectance spectra of APA membranes obtained in oxalic and sulphuric acid solution

the pore array of alumina, the asymmetric PL spectra can be assumed to be Gaussian [40] and it could be divided into two sub-bands as shown in Fig. 6a, b. Two Gaussian components of emission peaks, one at lower energy side corresponding to optical transitions in the F centers (oxygen vacancy with two electron), whereas another one at higher energy side originating from F⁺ centers (oxygen vacancy with one electron) was found in oxalic and sulphuric alumina. The maximum emission intensity (F centers) for oxalic and sulphuric alumina

was at 483 and 466 nm, which are near to middle of the blue region. On the other hand, lower emission intensity for oxalic and sulphuric alumina is at 423 and 421 nm, which are near to beginning of the blue region. Therefore, it is necessary to highlight that, in different electrolytes, such as oxalic and sulphuric alumina, PL spectra behavior of these membranes is in the same manner. From this, it may be concluded that the luminescence of anodic alumina depends on the type of the acid in electrolyte solution. Chromaticity analysis of PL spectra for oxalic and sulphuric alumina is shown in Fig. 6. The chromaticity coordinates obtained for oxalic (Fig. 6c) and sulphuric (Fig. 6d) were $x=0.1951, y=0.2033$ and $x=0.2075, y=0.2483$, respectively. From Fig. 6, it was observed that the maximum PL intensity of oxalic and sulphuric alumina has blue emission color. The intensity of PL peak is lower for sulphuric alumina than for membranes obtained in oxalic alumina. This could be due to the presence of oxalic impurities in the structure of APA in oxalic acid [41]. The structural and optical analysis data are tabulated in Table 1.

In the present work, micro-hardness of APA membranes was tested for 50 g in both oxalic and sulphuric alumina. The initial application of the force was set at 5 s and the test force was maintained for 15 s. The Vickers hardness was evaluated by the following expression [42]:

$$H_v = \frac{P}{A} = 1.85 \frac{P_{max}}{d^2} \tag{1}$$

Here, P represents the applied force to the diamond, A represents projected surface area of the indent, and d

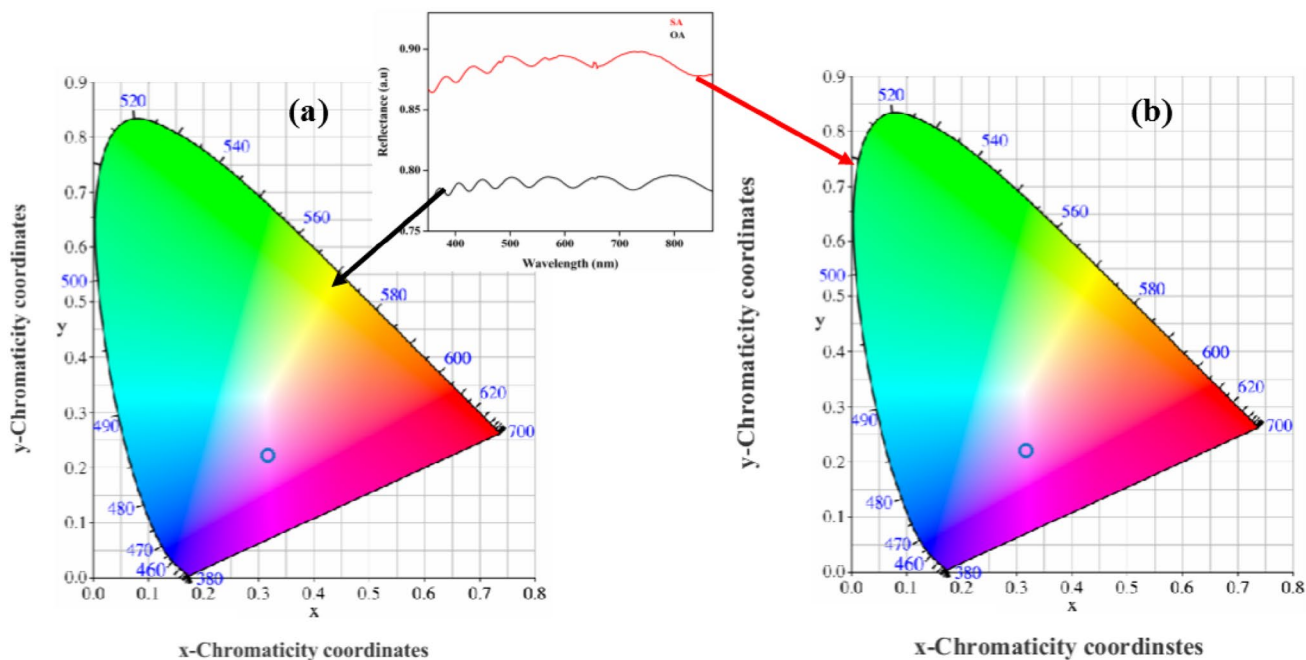


Fig. 5 CIE chromaticity diagram for reflectance spectra in **a** oxalic and **b** sulphuric alumina

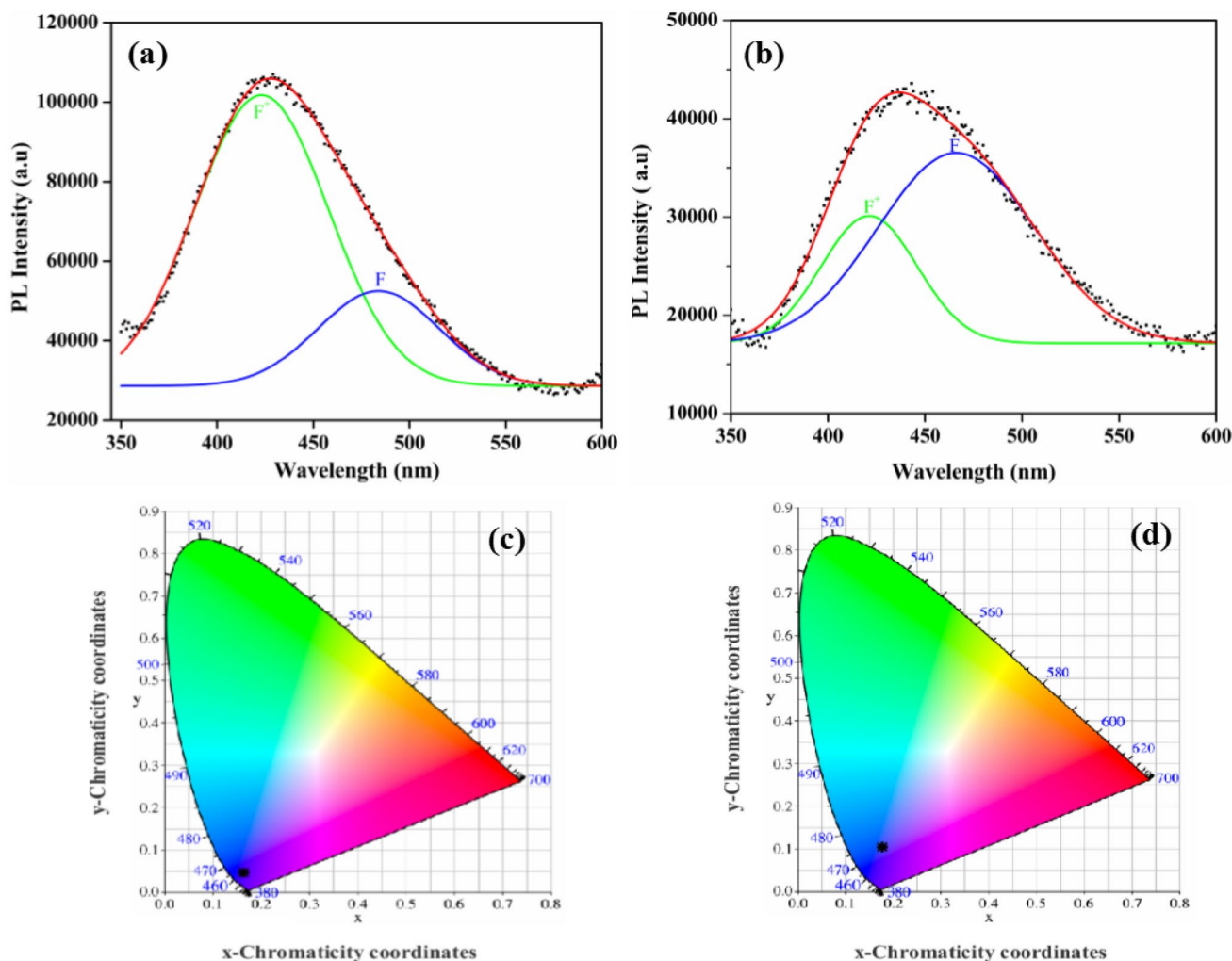


Fig. 6 PL spectra with Gaussian, separated into two sub-bands in oxalic (a) and sulphuric (b) alumina. Chromaticity diagram for PL spectra in oxalic and d sulphuric alumina

Table 1 Structural and optical data of oxalic and sulphuric alumina

Sample	Pore diameter (nm)	Interpore distance (nm)	Porosity (%)	Wall thickness (nm)	λ (nm)	$F^+-\lambda_1$ (nm)	$F-\lambda_2$ (nm)
OA	64	122	25	29	428	423	483
SA	34	69	22	17	436	421	466

represents average length of the indenter diagonal. Figure 7 shows the SEM micrograph of the Vickers indenter with a load of 50 g in oxalic (Fig. 7a, inset) and sulphuric alumina (Fig. 7b- inset), and the corresponding morphologies at the edges of the indenter are also shown in Fig. 7. The measured hardness values are 0.92 and 1.14 GPa correspondingly for oxalic and sulphuric alumina. It was noticed that porous formation was crushed during the indentation and suffered a crack along the pore wall in oxalic and sulphuric alumina. In fact, more number of cracks were observed in oxalic alumina (Fig. 7b) compared

with sulphuric alumina, due to high porosity (25%) and pore diameter of oxalic alumina [43]. The yield strength of alumina can be expressed as follows [42]:

$$\sigma = \frac{H_v}{c_v} \tag{2}$$

Here, c_v represents the geometrical factor, usually in the range of 2–4. The measured yield strengths of APA membranes by assumption that $C_v = 3$ are 0.38 and 0.30 GPa for oxalic and sulphuric alumina. Furthermore, to study the

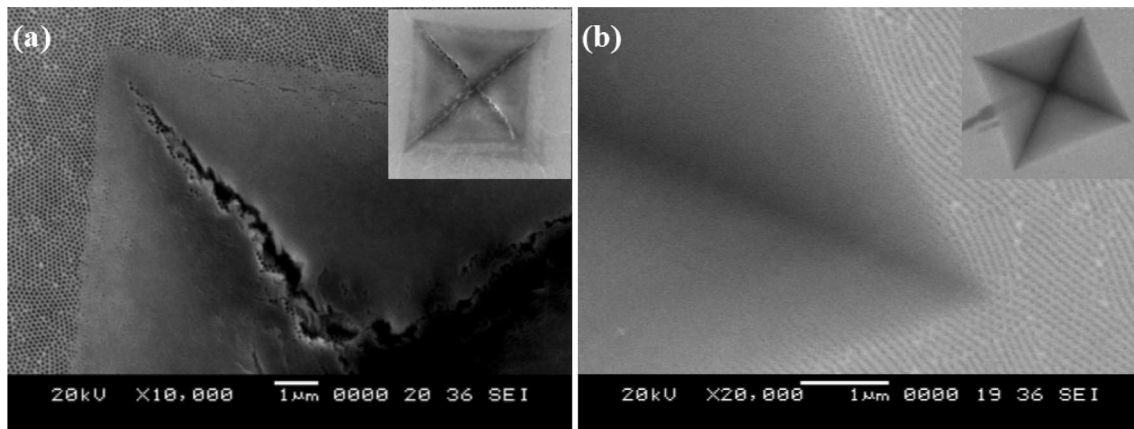


Fig. 7 SEM images of indented images of APA membranes after indentation by Vickers indenter and respective morphologies at the edge of the alumina with a load of 500 g in oxalic (a) and sulphuric (b) alumina

mechanical enhancement, we examined the hardness and Young's modulus of the APA membranes using Nanoindentation technique. Figure 8 shows the AFM images of the indented mark (7 mN) after indentation in oxalic (Fig. 8a) and sulphuric (Fig. 8b) alumina, respectively. The deformed material around the indents appeared free of cracks and a slight pile-up material occurred around the indent was noticed in oxalic and sulphuric alumina. The corresponding load–displacement curves of the APA membranes for indentation loads of 5, 7 mN are shown in Fig. 9. It was found that, with increasing load, the penetration depth also increases and no pop-in behavior occurs in oxalic (Fig. 9a) and sulphuric alumina (Fig. 9b). The elastic recovery can be calculated from the ratio of final depth of the indent (h_f), to the maximum depth of the indent (h_{max}). This ratio gives the significant indication of effect of pile-up, which can

influence the measurements of mechanical properties [44]. In the present study, the load displacement curves reveals that h_f/h_{max} for 7 mN were 0.66 and 0.73 for oxalic and sulphuric alumina. The elastic recovery (h_f/h_{max}) is decreased in oxalic alumina compared with sulphuric alumina, this is due to indenter penetration depth (h_{max}) is more in oxalic alumina. The nanohardness and Young's modulus for oxalic alumina were 3.76 and 85.85 GPa, whereas sulphuric alumina were 7.70 and 138.80 GPa, respectively. The nano hardness and Young's modulus of sulphuric alumina were more compared with those values in oxalic alumina, due to low porosity and regularity of the pores in sulphuric alumina [43].

Alumina nanowire (ANW) arrays were produced from APA membranes by chemical etching the samples in phosphoric acid solution [45], which is shown in Fig. 11. The

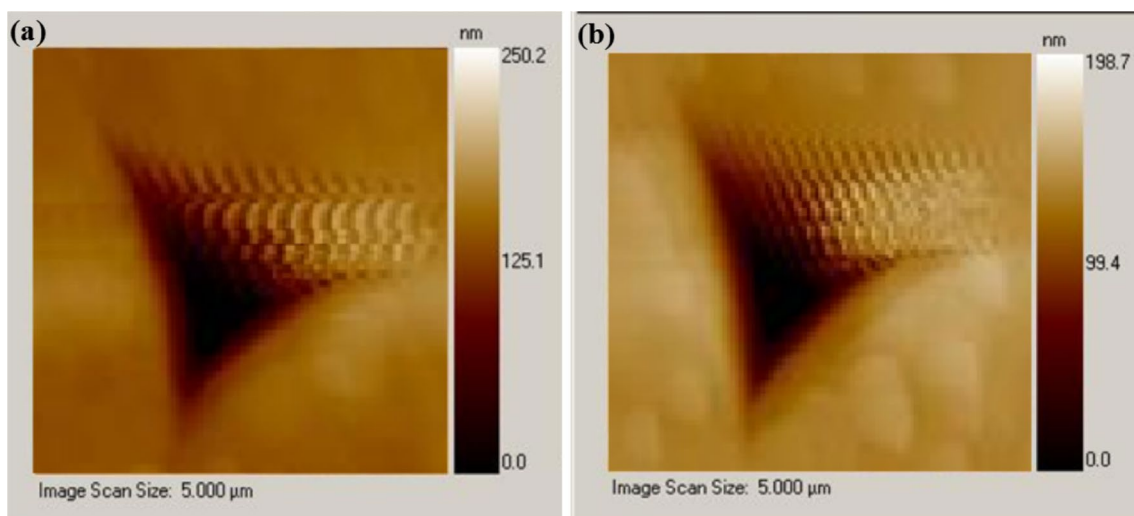


Fig. 8 AFM images of the nanoindentation imprints in oxalic (a) and sulphuric (b) alumina

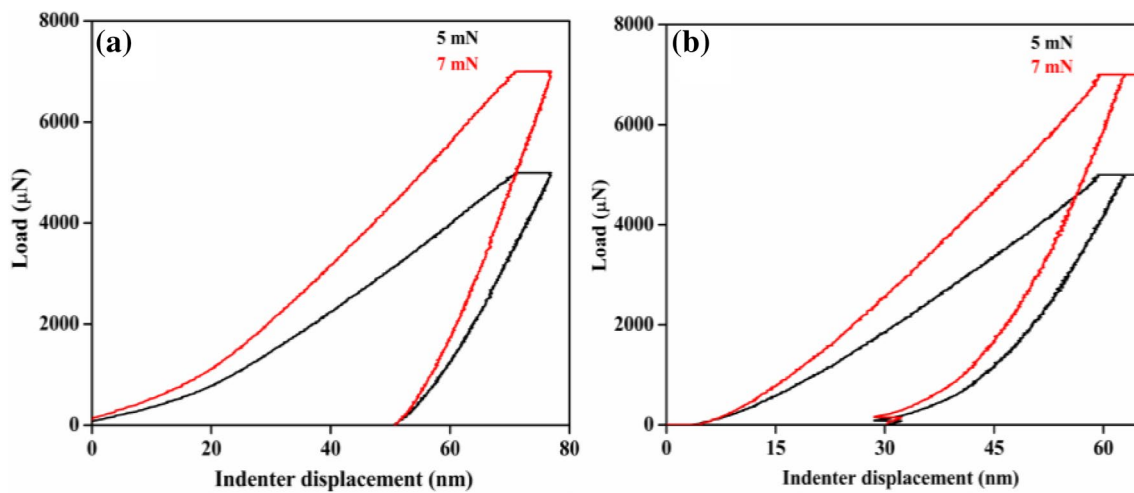


Fig. 9 Load–displacement curves of the APA membranes in formed in oxalic (a) and sulphuric (b) acid, respectively

schematic illustration of the formation of the ANW is shown in Fig. 10. Figure 10a shows the APA membranes with hexagonal array of pores, formed in 0.3 M of oxalic acid. During the dissolution of alumina membranes in phosphoric acid, pore walls linking three neighboring cells (triplet point) are thinning, as shown in Fig. 10b after the dissolution of 10 min. Further increasing etching time from 10 to 20 min, the thinning walls are broken, and triplet points are separated is shown in Fig. 10c. After 30 min, the pore walls are dissolved only nanowires remaining, which are generated from triplet points of the pores observed in oxalic (Fig. 11b) sulphuric alumina (Fig. 11a) respectively. Finally, after 45 min dissolution, the APA membrane is completely dissolved, and dense alumina nanowires were observed in oxalic (Fig. 11d) and sulphuric acid (Fig. 11c) with the same orientation. The thickness of the APA membranes can influence the result of the ANW. The nanowires have uniform diameter with a thickness less than 10 nm, and length is in below 5 μm in oxalic and sulphuric acid, which is related to the original

thickness of alumina membrane. The thickness of alumina increases with increasing the electrolyte concentration [46]. Formation of the ANW corresponds to the splitting of the wall surroundings of the pores. The number of pores on the surface of the APA membranes is larger, compared with the interface between the APA membrane and Al substrate [47]. It infers that the wall between the pores is thinner near to the surface compared with the beneath. Splitting between the pores is more likely to be near to the surface, because the pore density is high at near to the surface. The number of ANW array depends on the number of walls split, in our studies, the number of walls splitting is more in sulphuric alumina (Fig. 11c) compared with oxalic alumina (Fig. 11d), due to smaller wall thickness in sulphuric alumina (17 nm). Growth of nanostructures on the APA membranes itself without the need to implant materials is the significance of the present work. These ANW are suitable for applications in various fields, such as catalyst, electrolytic capacitors, and negative electrodes of Li-ion batteries [48].

Fig. 10 Schematic of the formation of the ANW from APA: **a** porous structure of the APA with triplet point, **b** thinning of pore walls after dissolution of APA in H_3PO_4 solution, and **c** alumina nanowires formation from triplet points

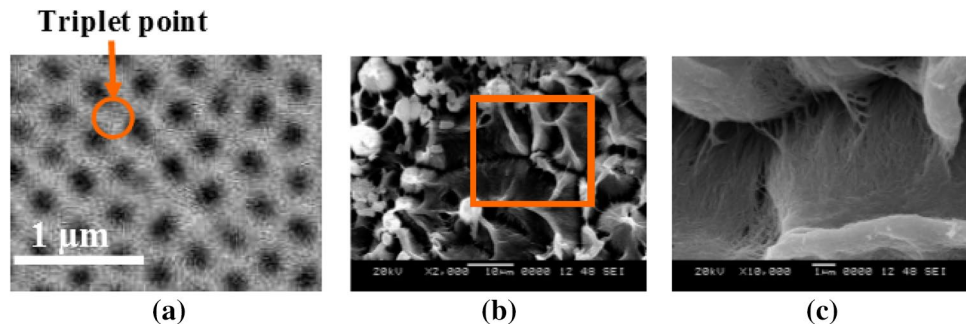
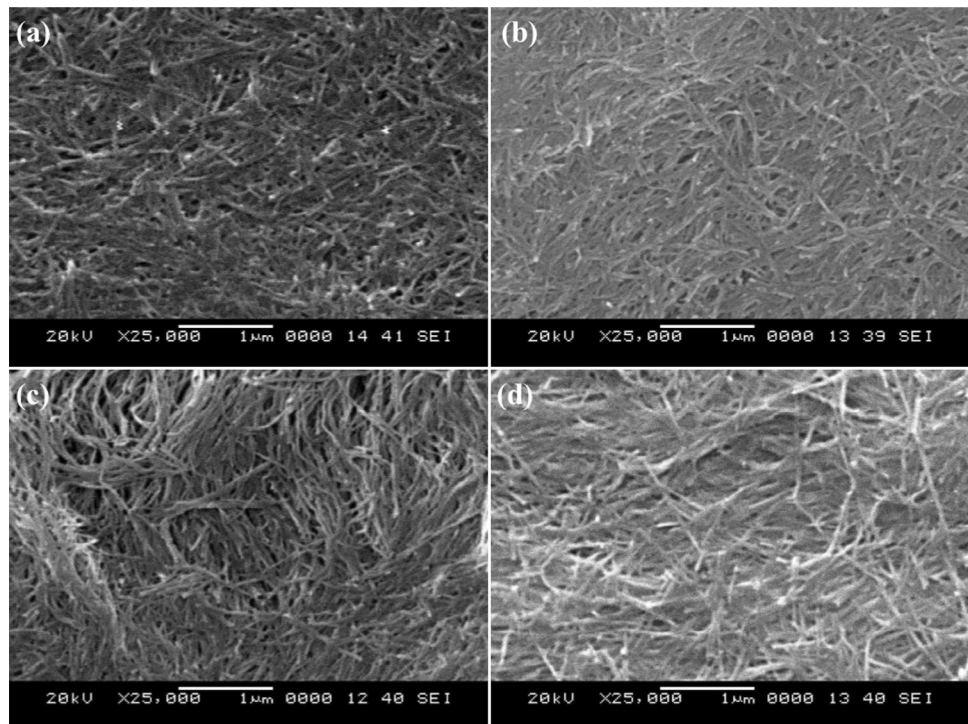


Fig. 11 SEM micrographs of the ANW formed in sulphuric and oxalic acid with the dissolution of APA membranes 30 (a, b) and 45 min (c, d) in H_3PO_4 solution



4 Conclusions

In summary, we have successfully prepared uniform order APA membranes using oxalic and sulphuric acid electrolytes by two-step anodization process. ANW were systematically fabricated on the pore channels of oxalic and sulphuric alumina using chemical etching method within a short period of time 45 min. Structural features of APA membranes were studied using the Image J software. Better pore ordering was noticed in oxalic alumina from regularity ratio measurements. XRD analyses show that as synthesized alumina in oxalic and sulphuric acid amorphous nature. The band-gap energy of APA membranes was determined from UV–visible absorption data. The maximum numbers of interference reflections were observed in oxalic alumina compared with sulphuric alumina because of large thickness of alumina in oxalic acid. The PL intensity of sulphuric alumina was less compared with oxalic alumina, due to oxalic impurities in the structure of oxalic alumina. PL studies of amorphous APA membranes reveals F and F^+ defect centers, which are attributed to oxygen vacancy-related defect centers in oxalic and sulphuric alumina. More cracks were formed in oxalic alumina from micro-indentation test, due to increase in pore diameter and porosity. The highest hardness and Young's modulus were observed in sulphuric alumina through nanoindentation test compared with oxalic alumina, due to low porosity and regularity of membranes formed in sulphuric acid. It was concluded that the wall thickness of the pores played the major role in the formation of ANW array.

The number of ANW array obtained in sulphuric alumina was more compared with that obtained from oxalic alumina because of smaller pore wall thickness in sulphuric alumina.

Acknowledgements The authors are thankful to Industrial Research & Consultancy Center, Indian Institute of Technology Bombay, India for supporting with the nanoindentation facility.

Funding The one of the author P. Ramana Reddy wishes to acknowledge MHRD for their financial support throughout the research work.

References

1. L. Zaraska, G.D. Sulka, M. Jaskula, J. Solid State Electrochem. **15**, 2427 (2011)
2. S. Mátéfi-Tempfli, M. Mátéfi-Tempfli, L. Piraux, Appl. Phys. A **96**, 603 (2009)
3. G.S. Huang, X.L. Wu, Y.C. Cheng, J.C. Shen, A.P. Huang, P.K. Chu, Appl. Phys. A **86**, 463 (2007)
4. A.I. Vorobjova, D.L. Shimanovich, E.A. Outkina, A.A. Khodin, Appl Phys A **124**, (2018)
5. Y. Peng, Q. Chen, Appl. Phys. A **105**, 841 (2011)
6. W.J. Stępniewski, M. Salerno, Fabrication of nanowires and nanotubes by anodic alumina template-assisted electrodeposition (One Central Press, Manchester, UK, 2014)
7. M. Ghrib, R. Ouertani, M. Gaidi, N. Khedher, M.B. Salem, H. Ezzaouia, Appl. Surf. Sci. **258**, 4995 (2012)
8. M.H. Rahimi, S. Saramad, S.H. Tabaian, S.P. Marashi, A. Zolfaghari, M. Mohammadalinezhad, Appl. Surf. Sci. **256**, 12 (2009)
9. A. Belwalkar, E. Grasing, W. Van Geertruyden, Z. Huang, W.Z. Misiolek, J. Membr. Sci. **319**, 192 (2008)
10. G.D. Sulka, W.J. Stępniewski, Electrochim. Acta **54**, 3683 (2009)
11. W.J. Stępniewski, Z. Bojar, Surf. Coat. Technol. **206**, 265 (2011)

12. A.K. Singh, B. Das, P. Sen, S.K. Bandopadhyay, K. Mandal, *IEEE Trans. Magn.* **50**, 1 (2014)
13. J. Sung, H. Moon, J.H. Bahng, J.-Y. Koo, B. Kim, in *MRS Proceedings* (Cambridge Univ Press, 2004), pp. M11–34
14. G.D. Sulka, L. Zaraska, W.J. Stepniowski, *Encycl. Nanosci. Nanotechnol.* **11**, 261 (2011)
15. A.K. Singh, K. Mandal, *J. Nanosci. Nanotechnol.* **14**, 5036 (2014)
16. A.K. Singh, K. Mandal, *J. Appl. Phys.* **117**, 105101 (2015)
17. D.A. Brevnov, G.R. Rao, G.P. López, P.B. Atanassov, *Electrochim. Acta* **49**, 2487 (2004)
18. J. Wang, C.-W. Wang, Y. Li, W.-M. Liu, *Thin Solid Films* **516**, 7689 (2008)
19. M. Serry, A. Gamal, M. Shaban, A. Sharaf, *IET Micro & Nano Letters* **8**, 775 (2013)
20. G.H. Li, Y. Zhang, Y.C. Wu, L.D. Zhang, *J. Phys.: Condens. Matter.* **15**, 8663 (2003)
21. A.P. Li, F. Müller, A. Birner, K. Nielsch, U. Gösele, *J. Appl. Phys.* **84**, 6023 (1998)
22. Z. Xia, L. Riemer, B.W. Sheldon, W.A. Curtin, J. Liang, A. Yin, J.M. Xu, *Rev. Adv. Mater. Sci.* **6**, 131 (2004)
23. K.Y. Ng, Y. Lin, A.H.W. Ngan, *Acta Mater.* **57**, 2710 (2009)
24. A.P. Samantilleke, J.O. Carneiro, S. Azevedo, T. Thuy, V. Teixeira, in *Journal of Nano Research* (Trans Tech Publ, 2013), pp. 77–89
25. G.G. Khan, A.K. Singh, K. Mandal, *J. Lumin.* **134**, 772 (2013)
26. K.S. Choudhari, P. Sudheendra, N.K. Udayashankar, *J. Porous Mater.* **19**, 1053 (2012)
27. P.R. Reddy, K.M. Ajith, N.K. Udayashankar, *Ceram. Int.* **42**, 17806 (2016)
28. L. Zaraska, W.J. Stepniowski, G.D. Sulka, E. Ciepiela, M. Jaskuła, *Appl. Phys. A* **114**, 571 (2014)
29. P.R. Reddy, K.M. Ajith, N.K. Udayashankar, *J. Mater. Sci.: Mater. Electron.* **27**, 5331 (2016)
30. W.J. Stepniowski, J. Choi, H. Yoo, M. Michalska-Domańska, P. Chilimoniuk, T. Czujko, *Mater. Lett.* **164**, 176 (2016)
31. F. Laatar, M. Hassen, C. Amri, F. Laatar, A. Smida, H. Ezzaouia, *J. Lumin.* **178**, 13 (2016)
32. F. Majid, T. Ijaz, M. Farooq, S. Riaz, S. Naseem, in *Proc. 2013 World Congress on Advances in Nano, Biomechanics, Robotics and Energy Research (ANBRE)* (2013)
33. I.A. Vrublevsky, K.V. Chernyakova, A. Ispas, A. Bund, S. Zavadski, *Thin Solid Films* **556**, 230 (2014)
34. W.J. Stepniowski, J. Choi, H. Yoo, K. Oh, M. Michalska-Domańska, P. Chilimoniuk, T. Czujko, R. Lyszkowski, S. Józwiak, Z. Bojar, and others. *J. Electroanal. Chem.* **771**, 37 (2016)
35. W.J. Stepniowski, M. Norek, B. Budner, M. Michalska-Domańska, A. Nowak-Stepniowska, A. Bombalska, M. Kaliszewski, A. Mostek, S. Thorat, M. Salerno, et al. *Thin Solid Films* **598**, 60 (2016)
36. M. Shaban, *J. Spectrosc.* 2016, (2016)
37. H.M. Chen, C.F. Hsin, R.-S. Liu, S.-F. Hu, C.-Y. Huang, *J. Electrochem. Soc.* **154**, K11 (2007)
38. J. Li, Z. Zhu, Y. Hu, J. Zheng, J. Chu, W. Huang, *J. Nanomater.* **2014**, 51 (2014)
39. A. Santos, M. Alba, M.M. Rahman, P. Formentín, J. Ferré-Borrull, J. Pallarès, L.F. Marsal, *Nanoscale Res. Lett.* **7**, 1 (2012)
40. G.S. Huang, X.L. Wu, L.W. Yang, X.F. Shao, G.G. Siu, P.K. Chu, *Appl. Phys. A* **81**, 1345 (2005)
41. G. Tao, M. Guo-Wen, Z. Li-De, *Chin. Phys. Lett.* **20**, 713 (2003)
42. T.-H. Fang, T.H. Wang, C.-H. Liu, L.-W. Ji, S.-H. Kang, *Nanoscale Res. Lett.* **2**, 410 (2007)
43. N. Tsyntsar, B. Kavas, J. Sort, M. Urgen, J.-P. Celis, *Mater. Chem. Phys.* **148**, 887 (2014)
44. G. Alcalá, P. Skeldon, G.E. Thompson, A.B. Mann, H. Habazaki, K. Shimizu, *Nanotechnology* **13**, 451 (2002)
45. J.K. Han, J. Kim, Y.C. Choi, K.-S. Chang, J. Lee, H.J. Youn, S.D. Bu, *Physica E: Low-Dimens. Syst. Nanostruct.* **36**, 140 (2007)
46. C.H. Voon, M.N. Derman, in *Advanced Materials Research* (Trans Tech Publ, 2013), pp. 610–614
47. Y.F. Mei, G.G. Siu, R.K. Fu, P. Chen, X.L. Wu, T.F. Hung, P.K. Chu, Y. Yang, *J. Appl. Phys.* **97**, 034305 (2005)
48. T. Kondo, N. Kitagishi, T. Fukushima, T. Yanagishita, H. Masuda, *Mater. Express* **6**, 363 (2016)